J|A|C|S
ARTICLES
Published on Web 12/08/2006

Model for Proton Transport Coupled to Protein Conformational Change: Application to Proton Pumping in the Bacteriorhodopsin Photocycle

Antonio M. Ferreira and Donald Bashford*

Contribution from the Department of Molecular Biotechnology, Hartwell Center for Bioinformatics and Biotechnology, St. Jude Children's Research Hospital, 332 North Lauderdale Street, Memphis, Tennessee 38105

Received January 31, 2006; E-mail: Don.Bashford@stjude.org

Abstract: A modeling method is presented for protein systems in which proton transport is coupled to conformational change, as in proton pumps and in motors driven by the proton-motive force. Previously developed methods for calculating pK_a values in proteins using a macroscopic dielectric model are extended beyond the equilibrium case to a master-equation model for the time evolution of the system through states defined by ionization microstate and a discrete set of conformers. The macroscopic dielectric model supplies free energy changes for changes of protonation microstate, while the method for obtaining the energetics of conformational change and the relaxation rates, the other ingredients needed for the master equation, are system dependent. The method is applied to the photoactivated proton pump, bacteriorhodopsin, using conformational free energy differences from experiment and treating relaxation rates through three adjustable parameters. The model is found to pump protons with an efficiency relatively insensitive to parameter choice over a wide range of parameter values, and most of the main features of the known photocycle from very early M to the return to the resting state are reproduced. The boundaries of these parameter ranges are such that short-range proton transfers are faster than longer-range ones, which in turn are faster than conformational changes. No relaxation rates depend on conformation. The results suggest that an "accessibility switch", while not ruled out, is not required and that vectorial proton transport can be achieved through the coupling of the energetics of ionization and conformational states.

1. Introduction

Ion transport across cellular membranes is ubiquitous in biological systems and of central importance to our understanding of cellular function. Mitchell's theory of chemiosmotic coupling[1] rests on the idea that protein systems use the cell's energy sources to actively transport protons across a membrane. This creates a chemical potential in the form of an electrochemical gradient or proton-motive force, which is used in subsequent reactions to drive the production of ATP from ADP via the action of ATP synthase.

Bacteriorhodopsin (bR), from the bacterium *Halobacterium salinarium*, is the smallest known autonomous light-driven proton pump and is responsible for the vectorial motion of protons from the cytoplasm to the extracellular side of the membrane following illumination. After nearly three decades of biophysical, spectroscopic, and structural studies, it is arguably the best-characterized proton pump in biology.[2−10] Net transfer of protons across the membrane proceeds in a stepwise fashion through several intermediates as shown in Figure 1. These intermediates are conventionally identified by time-resolved measurements of their visible absorption, which is dominated by changes in or near the chromophore, a retinal moiety linked to Lys216 by a Schiff base. The identity of the amino-acid residues on the proton-transfer pathway and the changes in their ionization states during the photocycle have been established mainly by time-resolved FTIR measurements.[11−13] An atomic structural model of bR based on electron diffraction studies[14] was among the earliest structures of membrane proteins and, later, high-resolution X-ray crystallographic structures of bR in the resting state were determined.[15−19] In addition, structural models for photocycle intermediates have been put

(1) Mitchell, P. *Nature* **1961**, *191*, 144−148.
(2) Heberle, J. *Biochim. Biophys. Acta* **2000**, *1458*, 135−147.
(3) Neutze, R.; Pebay-Peyroula, E.; Edman, K.; Royant, A.; Navarro, J.; Landau, E. M. *Biochim. Biophys. Acta* **2002**, *1565*, 144−167.
(4) Lanyi, J. K.; Pohorille, A. *Trends Biotechnol.* **2001**, *19*, 140−144.
(5) Balashov, S. P. *Biochim. Biophys. Acta* **2000**, *1460*, 75−94.
(6) Betancourt, F. M. H.; Glaeser, R. M. *Biochim. Biophys. Acta* **2000**, *1460*, 106−118.
(7) Haupts, U.; Tittor, J.; Oesterhelt, D. *Annu. Rev. Biophys. Biomol. Struct.* **1999**, *28*, 367−399.
(8) Hirai, T.; Subramaniam, S. *FEBS Lett.* **2003**, *545*, 2−8.
(9) Lanyi, J. K.; Luecke, H. *Curr. Opin. Struct. Biol.* **2001**, *11*, 415−419.
(10) Subramaniam, S. *Curr. Opin. Struct. Biol.* **1999**, *9*, 462−468.
(11) Rothschild, K. J. *J. Bioenerg. Biomembr.* **1992**, *24*, 147−167.
(12) Maeda, A. *Isr. J. Chem.* **1995**, *35*, 387−400.
(13) Kötting, C.; Gerwert, K. *ChemPhysChem* **2005**, *6*, 881−888.
(14) Henderson, R.; Baldwin, J. M.; Ceska, T. A.; Zemlin, F.; Beckmann, E.; Downing, K. H. *J. Mol. Biol.* **1990**, *213*, 899−929.
(15) Pebay-Peyroula, E.; Rummel, G.; Rosenbusch, J. P.; Landau, E. M. *Science* **1997**, *277*, 1676−1681.
(16) Luecke, H.; Richter, H.-T.; Lanyi, J. K. *Science* **1998**, *280*, 1934−1937.
(17) Essen, L.-O.; Siegert, R.; Lehmann, W. D.; Oesterhelt, D. *Proc. Natl. Acad. Sci. U.S.A.* **1998**, *95*, 11673−11678.
(18) Belrhali, H.; Nollert, P.; Royant, A.; Menzel, C.; Rosenbusch, J. P.; Landau, E. M.; Pebay-Peyroula, E. *Struct. Fold. Des.* **1999**, *7*, 909−917.
(19) Luecke, H.; Schobert, B.; Richter, H.-T.; Cartailler, J.-P.; Lanyi, J. K. *J. Mol. Biol.* **1999**, *291*, 899−911.

10.1021/ja060742d CCC: $33.50

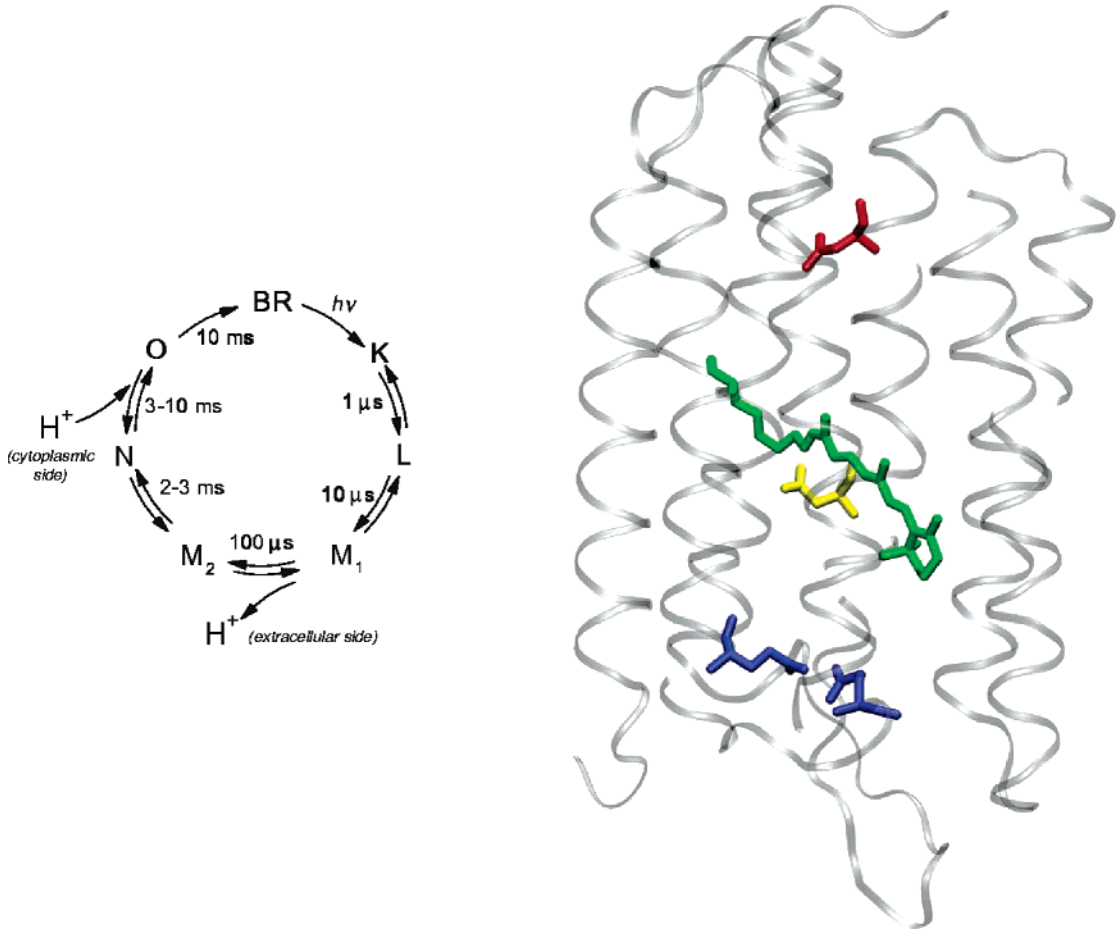

Figure 1. Schematic diagram of the bacteriorhodopsin photocycle (left) and the key residues involved in the proton translocation process (right). Absorption of a photon by the retinal chromophore in the light-adapted resting state (BR) leads to an electronically excited-state and an all-*trans* to 13-*cis* isomerization of the retinal chromophore and subsequent structural rearrangements (K → M). In M, a proton is transferred from the retinal's Schiff base linkage (green) to Asp85 (yellow) and simultaneously, a proton is released from the release group (blue) to the extracellular membrane surface. During the conformational change to N, the Schiff base is reprotonated from Asp96 (red). Reprotonation of Asp96 initiates a structural rearrangement to O. Finally, O decays to BR with reprotonation of the Schiff base from Asp85, restoring the initial state.

forward on the basis of crystallographic and electron diffraction work on mutant or wild-type bR trapped under various conditions.[20−31]

Despite the wealth of experimental data concerning the various intermediates in the bR photocycle and extensive kinetic measurements conducted for native and mutant proteins, there is still considerable debate over the exact mechanism. The current debate centers around two models for proton pumping. One view, the accessibility switch model,[7,32] proposes changes in the accessibility of various protonation sites with changes of conformations during the photocycle. Pumping occurs because the sequence of conformational changes opens and closes proton-transfer pathways between sites in a coordinated manner. The other view, the affinity switch or local access model,[33,34] focuses on varying proton affinities among the ionizable groups, as represented by the pK_a values, rather than the opening or closing of access. Moreover, changes in the protonation states of the various residues play an important role in driving conformational changes.

The majority of computational studies of the bR photocycle have concentrated either on the resting state or the initial photochemical event leading to the isomerization of the Schiff base, and some studies have been done on the proton-transfer steps. Computational studies based on the new structural data have included calculations on the resting (BR) state,[35−38]

(20) Luecke, H.; Schobert, B.; Richter, H.-T.; Cartailler, J. P.; Lanyi, J. K. *Science* **1999**, *286*, 255−261.
(21) Edman, K.; Nollert, P.; Royant, A.; Belrhali, H.; Pebay-Peyroula, E.; Hajdu, J.; Neutze, R.; Landau, E. M. *Nature* **1999**, *401*, 822−826.
(22) Sass, H. J.; Büldt, G.; Gessenich, R.; Hehn, D.; Neff, D.; Schlesinger, R.; Berendzen, J.; Ormos, P. *Nature* **2000**, *406*, 649−653.
(23) Luecke, H.; Schobert, B.; Cartailler, J.-P.; Hans-Thomas, R.; Rosengarth, A.; Needleman, R.; Lanyi, J. K. *J. Mol. Biol.* **2000**, *300*, 1237−1255.
(24) Subramaniam, S.; Henderson, R. *Nature* **2000**, *406*, 653−657.
(25) Royant, A.; Edman, K.; Ursby, T.; Pebay-Peyroula, E.; EM, L.; Neutze, R. *Nature* **2000**, *406*, 645−648.
(26) Facciotti, M. T.; Rouhani, S.; Burkard, F. T.; Betancourt, F. M.; Downing, K. H.; Rose, R. B.; McDermott, G.; M, G. R. *Biophys. J.* **2001**, *81*, 3442−55.
(27) Rouhani, S.; Cartailler, J.; Facciotti, M.; Walian, P.; Needleman, R. Lanyi, J.; Glaeser, R.; Luecke, H. *J. Mol. Biol.* **2001**, *313*, 615−628.
(28) Schobert, B.; Cupp-Vickery, J.; Hornak, V.; Smith, S. O.; Lanyi, J. K. *J. Mol. Biol.* **2002**, *321*, 715−726.
(29) Lanyi, J. K.; Schobert, B. *J. Mol. Biol.* **2002**, *321*, 727−737.
(30) Lanyi, J. K.; Schobert, B. *J. Mol. Biol.* **2003**, *328*, 439−450.
(31) Schobert, B.; Brown, L. S.; Lanyi, J. K. *J. Mol. Biol.* **2003**, *330*, 553−570.
(32) Ormos, P. *Proc. Natl. Acad. Sci. U.S.A.* **1991**, *88*, 473−477.
(33) Richter, H.-T.; Brown, L. S.; Needleman, R.; Lanyi, J. K. *Biochemistry* **1996**, *35*, 4054−4062.
(34) Brown, L. S.; Dioumaev, A. K.; Needleman, R.; Lanyi, J. K. *Biophys. J.* **1998**, *75*, 1455−1465.
(35) Spassov, V. Z.; Luecke, H.; Gerwert, K.; Bashford, D. *J. Mol. Biol.* **2001**, *312*, 203−219.
(36) Baudry, J.; Tajkhorshid, E.; Molnar, F.; Phillips, J.; Schulten, K. *J. Phys. Chem. B* **2001**, *105*, 905−918.

dynamics studies of early rapid steps prior to any proton transport,[36,39,40] and events in the M intermediate.[41,42] Calculations using a macroscopic dielectric model of the protein/membrane/solvent system and solutions of the corresponding Poisson or Poisson−Boltzmann equations by ourselves and others have provided predictions of the ionization states of the key residues in agreement with experiment[43−45] and given support to the hypothesis that the proton initially released to the extracellular side is stored in a hydrogen-bonded water network within the protein.[35,46] Song et al.[47] have made pK_a calculations at different substates of M using several of the new X-ray structures.

Recently, we presented macroscopic dielectric calculations of the energetics of different protonation states in structural models of the M, N, and O states as well as in the resting (BR) state and combined these with a set of accessibility rules to reason about possible allowed, energetically downhill proton-transfer steps.[48] A limitation was that the conformational changes, M → N → O → BR were simply assumed; in other words, a "forced march" through these conformers was imposed. A goal of the present work is to go beyond both the limitations of equilibrium-based methods and the assumption of a forced march in a model for the time-dependent behavior of bR as it pumps protons.

Master-equation methods[49] have been used to study complex chemical kinetics in several areas of chemistry such as combustion,[50] atmospheric chemistry,[51] and diffusion-limited reactions.[52] A master-equation-like approach also has been used together with empirical valence bond methods to study proton movement along H-bonded "wires" in the photosynthetic reaction center.[53]

Starting from techniques used in macroscopic electrostatic calculations to determine equilibrium ionization states and pK_a values, we have developed extensions for modeling the non-equilibrium time-dependent behavior of proton pumps driven by conformational change, or conversely, motors driven by the proton-motive force. A discrete master-equation approach is used in which the microstates are defined by ionization state and conformation, and the overall proton transport process can be described as a series of elementary steps involving either the transfer of a single proton between two ionizable sites or between an ionizable site and the bulk, or a protein conformational change. Ratios of rates for each possible proton-transfer depend on free energy differences, which are determined by Poisson−Boltzmann calculations of the same kind used for pK_a prediction in proteins.[54] In the present application to bR, free energy differences for conformational change are based on experimental measurements. The remaining information needed to determine the master-equation rate matrix are relaxation rates. In this context, the affinity switch versus accessibility switch question can be framed as a question of whether these relaxation rates vary with protein conformation or ionization changes (with increases and decreases corresponding to the opening and closing of access in the accessibility switch model). We explore a null hypothesis with respect to changes in accessibility by assuming *no* variation in relaxation rate and ask whether vectorial proton pumping can be achieved simply by the coupling of ionization energetics with conformation, and whether the resulting model photocycles resemble those determined experimentally. This hypothesis corresponds to a pure affinity switch model. The sensitivity of the model to a broad range of choices for the (fixed) relaxation rates is explored.

The approach presented is generalizable to many transport processes that can be described as a combination of simple transfers of ligands between chemically isolated sites in a larger macromolecule and conformational changes in that macromolecule. For the case of bR, the ligand is the proton, and the sites are the ionizable moieties of the proton, but more generally the ligands can be electrons, ions, or small molecules and the sites redox centers or a collection of binding pockets in a large protein. Atomic structural models for the macromolecule and its conformational repertoire are needed, thus the method may find wider applicability as more membrane protein structures are determined.

2. Theory

2.1. Rate Matrix. A first-order kinetics, or master-equation approach[49] includes the designation of discrete microstates and the master equation:

$$\frac{\mathrm{d}p_i(t)}{\mathrm{d}t} = \sum_{j=1}^{N_\mathrm{m}} R_{ij}\, p_j(t) \qquad (1)$$

where $p_i(t)$ is the probability of finding the system in state i at time t, R_{ij} is the probability per unit time that a molecule in state j will make a transition to state i, and N_m is the number of microstates. We will use italics (e.g., p_i) to designate the probability of a single microstate and boldface (e.g., $\boldsymbol{p}$) to designate the vector of microstate probabilities. Thus, $\boldsymbol{p}(t)$ contains all microstate probabilities at some time t. The diagonal elements, R_{ii}, are determined by conservation of matter:

$$R_{ii} = -\sum_{k \neq i} R_{ki} \qquad (2)$$

The solution of eq 1 is described in section 2.4, but the first task is to define the microstates and the nature of the transitions between them. The key events in conformationally driven transmembrane proton transport are proton transfer from one site within the protein to another, transfer between the bulk on a specific side of the membrane and specific sites in the protein,

(37) Rajamani, R.; Gao, J. L. *J. Comput. Chem.* **2002**, *23*, 96−105.
(38) Vreven, T.; Morokuma, K. *Theor. Chem. Acc.* **2003**, *109*, 125−132.
(39) Hayashi, S.; Tajkhorshid, E.; Schulten, K. *Biophys. J.* **2002**, *83*, 1281−1297.
(40) Hayashi, S.; Tajkhorshid, E.; Schulten, K. *Biophys. J.* **2003**, *85*, 1440−1449.
(41) Grudinin, S.; Büldt, G.; Gordeliy, V.; Baumgaertner, A. *Biophys. J.* **2005**, *88*, 3257−3261.
(42) Bondar, A.-N.; Elstner, M.; Suhai, S.; Smith, J. C.; Fischer, S. *Structure* **2004**, *12*, 1281−1288.
(43) Bashford, D.; Gerwert, K. *J. Mol. Biol.* **1992**, *224*, 473−486.
(44) Sampogna, R. V.; Honig, B. *Biophys. J.* **1994**, *66*, 1341−1352.
(45) Engels, M.; Gerwert, K.; Bashford, D. *Biophys. Chem.* **1995**, *56*, 95−104.
(46) Rammelsberg, R.; Huhn, G.; Lübben, M.; Gerwert, K. *Biochemistry* **1998**, *37*, 5001−5009.
(47) Song, Y.; Mao, J.; Gunner, M. R. *Biochemistry* **2003**, *42*, 9875−9888.
(48) Onufriev, A.; Smondyrev, A.; Bashford, D. *J. Mol. Biol.* **2003**, *332*, 1183−1193.
(49) van Kampen, N. G. *Stochastic Processes in Physics and Chemistry*; North-Holland: Amsterdam, 1981; Chapter V.
(50) Pilling, M. J.; Robertson, S. H. *Ann. Rev. Phys. Chem.* **2003**, *54*, 245−275.
(51) Barker, J. R.; Golden, D. M. *Chem. Rev.* **2003**, *103*, 4577−4591.
(52) Mattis, D. C.; Glasser, M. L. *Rev. Mod. Phys.* **1998**, *70*, 979−1001.
(53) Sham, Y. Y.; Muegge, I.; Warshel, A. *Proteins: Struct. Funct. Genet.* **1999**, *36*, 484−500.
(54) Bashford, D.; Karplus, M. *Biochemistry* **1990**, *29*, 10219−10225.

and protein conformational changes. We therefore choose a specification of the proton occupancy of key sites and a discrete set of conformational states as the descriptors of the microstates. If the model contains c possible conformers and s sites, each of which can be in one of two states (protonated or deprotonated), the number of microstates is simply $N_m = c2^s$. This places some practical bounds on the number of sites and conformers and, therefore, the number of microstates to be included in the model. We take the elementary transitions to be of two types: (1) conformational changes and (2) single proton-transfer events, which may either be between two sites or between a site and the bulk on one side of the membrane or the other. Not all pairs of sites are directly accessible to each other, and not all sites are accessible to the bulk. In particular, in the present model, no sites are directly accessible to both sides of the membrane. For example, proton transfers between the Schiff base and the extracellular or cytoplasmic bulk are accomplished by a series of transfers involving the other residues. These elementary steps are the only allowed transitions. Although one can imagine concerted steps, such as simultaneous motion of multiple protons or conformational change combined with proton transfer, we exclude such complications from the current model. The transition matrix will be sparse thanks to these restrictions, and much of the information for determining the values of nonzero elements is given by the relative free energies of the states. For a given conformer, these energies are determined from electrostatics calculations (see section 2.2) while the relative free energies of the conformers are obtained from experimental data.

The principle of detailed balance requires that if the system is at equilibrium and $\boldsymbol{p}^{eq}$ are the equilibrium values of $\boldsymbol{p}$, then

$$R_{ij}\, p_j^{eq} = R_{ji}\, p_i^{eq} \tag{3}$$

Therefore, the rates may be related to the free energy differences, ΔG_{ij}, between microstates according to

$$R_{ij} = \frac{\kappa_{ij}}{1 + e^{-\beta \Delta G_{ij}}} \tag{4}$$

where $\kappa_{ij} = \kappa_{ji} = R_{ij} + R_{ji}$ is a relaxation rate for the $i \leftrightarrow j$ process. Thus, the full rate matrix is determined by the transition rules (which determines which elements are zero), the relative free energies of the states, and the relaxation rates.

The relaxation rates κ, appearing in eq 4, are not interpreted as exchange rates as measured, for example, by H/D exchange. The physical meaning of κ is that if the two states i and j were isolated from any other state transitions and their population was disturbed from equilibrium, then κ would the rate at which the system would relax back to equilibrium. In the case of large $|\beta\Delta G|$, κ is the limiting rate of the faster of the forward or backward rates. In contrast, exchange rates are dominated by the slower of the two rates.

Methods to calculate the ΔG are described below, but there remains the problem of determining the relaxation rates κ. In principle, this could be done by calculation of barrier heights for proton transfer, etc., but the present study is focused on broad questions of how relative rates for different kinds of events affect pumping or whether certain transitions need to be shut off ($\kappa = 0$) or turned on at different points in the photocycle for vectorial proton transport. We therefore divide elementary steps into categories and regard the κ values assigned to them as adjustable parameters.

2.2. Energetics. An extension of our previous work on pK_a and conformational change in proteins[54,55] is used to obtain the free energy differences needed for the non-zero R_{ij} elements. It is convenient to handle binding state changes and conformational changes on the same footing, so we regard conformational changes as unimolecular interconversions of different "chemical" species and write the following expression for the chemical potential of a molecule with N proton-binding sites as a function of the binding and conformational microstate, in which $\boldsymbol{x}$ is an N-element vector of labels x_i, which specify the protonation state of the ith site in a particular microstate, and c labels the conformation:

$$\mu^\circ_M(c, \boldsymbol{x}) = E_g(c) + \sum_{i=1}^{N} P_i(c, x_i) + \frac{1}{2}\sum_{i=1}^{N}\sum_{j\neq i}^{N} W_{ij}(c, x_i, x_j) \tag{5}$$

The P and W are additive one-site and two-site terms describing the energetics of protonation (and its dependence on conformation, through c) while E_g describes the purely conformational energy component. The free energy change with a change of protonation state, $\boldsymbol{x} \rightarrow \boldsymbol{y}$ is

$$\Delta G(\boldsymbol{x} \rightarrow \boldsymbol{y}) = \mu^\circ_M(c, \boldsymbol{y}) - \mu^\circ_M(c, \boldsymbol{x}) - \Delta\nu(\boldsymbol{x} \rightarrow \boldsymbol{y})\mu_{H^+} \tag{6}$$

where $\Delta\nu$ is the change in the number of protons bound to the macromolecule, and μ_{H^+} is the proton chemical potential. Using the relation of proton chemical potential to pH, the more familiar intrinsic pK of protein titration theory[43,54,56,57] can be related to the P of eq 5:

$$-2.3\beta^{-1}\mathrm{p}K_{\mathrm{int},i}(c) = P_i(c, \mathrm{prot}) - P_i(c, \mathrm{deprot}) - \mu^\circ_{H^+} \tag{7}$$

where $\mu^\circ_{H^+}$, the standard chemical potential of the proton, is a constant that falls out of any actual calculation. The W in eq 5 are the same as those of the more familiar theory, and the free energy change associated with elementary proton-transfer steps can now be written explicitly in terms of pK_{int} and W. For a proton transfer between site i and the bulk, let $\boldsymbol{x}$ now be a vector specifying protonation states of sites other than i while protonated or deprotonated states of site i are indicated with p or d. The free energy change is

$$\Delta G(c, \boldsymbol{x}; \mathrm{bulk} \rightarrow i) = -2.3\beta^{-1}(\mathrm{p}K_{\mathrm{int},i}(c) - \mathrm{pH}_s) + \left[\sum_{k\neq i}^{N} W_{ik}(c, p_i, x_k) - W_{ik}(c, d_i, x_k)\right] \tag{8}$$

where pH_s is the pH on side s of the membrane. The site-to-bulk terms are the only kind of terms that are pH dependent.

(55) Spassov, V. Z.; Bashford, D. *J. Comput. Chem.* **1999**, *20*, 1091−1111.
(56) Tanford, C.; Kirkwood, J. G. *J. Am. Chem. Soc.* **1957**, *79*, 5333−5339.
(57) Yang, A.-S.; Gunner, M. R.; Sampogna, R.; Sharp, K.; Honig, B. *Proteins* **1993**, *15*, 252−265.

For a proton transfer between two sites, i and j, the expression is somewhat more complex:

$$\Delta G(c, \mathbf{x}; j \rightarrow i) = -2.3\beta^{-1}[\mathrm{p}K_{\mathrm{int},i}(c) - \mathrm{p}K_{\mathrm{int},j}(c)] + \left[\sum_{k\neq i,j}^{N} W_{ik}(c, p_i, x_k) - W_{ik}(c, d_i, x_k) - W_{jk}(c, p_j, x_k) + W_{jk}(c, d_j, x_k)\right] + W_{ij}(c, p_i, d_j) - W_{ij}(c, d_i, p_j) \quad (9)$$

All ΔG values corresponding to proton transfers can be derived from a set of $\mathrm{p}K_{\mathrm{int}}$ and W_{ij} values for the various sites for each of the c conformers of the protein. These can in turn be obtained by the usual kind of macroscopic electrostatic calculations, as described in section 3. Finally, the purely conformational term of eq 5 (E_g for each of the c conformations) can be determined if one knows the free energy of some set of $c - 1$ conformational changes with a fixed protonation that connect all the conformers. In the present case, these are drawn from the experimental literature (see section 3).

2.3. Merged Sites and Rapid Equilibrium. In some cases, including the present application, there may be ionizable sites clustered very closely together that can share one or more protons via proton transfers much more rapidly than the time scale of interest for the overall system. In these cases, numerical difficulties related to many order-of-magnitude rate differences can be avoided, and the number of sites in the model can be reduced by regarding such complexes as a single site which is always in *internal* equilibrium. Suppose the last m of the N sites are to be merged, so the new site index will be $N' = N - m + 1$. The merged but not-yet-equilibrated site will have all possible combinations of its subsites states; for example, merging three sites that each have two states, protonated and deprotonated, will give a single merged site with 2^3 states, one with no protons, three with one proton, three with two protons, and one with three protons. The expression for standard chemical potential of the system with the merged site is

$$\mu^\circ = \sum_{i=1}^{N'-1} P_i(x_i) + \frac{1}{2}\sum_{i,j=1}^{N'-1} W_{ij}(x_i, x_j) + P_{N'}(y) + \sum_{i=1}^{N'-1} W_{i,N'}(x_i, y) \quad (10)$$

where y labels the states of the merged site N', and the conformational dependence is omitted for brevity. The construction of $P_{N'}$ and the $W_{i,N'}$ involves straightforward sums over terms related to the sites being merged together.

The assumption of a very rapid internal proton exchange implies that states of the merged site having the same number of protons are in thermal equilibrium with each other. For each possible number of protons, υ, in the merged site, there will be a corresponding set of merged-site states, s_μ, which will become a singe state, which we label as z_υ. The new expression for chemical potential in terms of z_υ is given by a thermodynamic summation over the states in s_υ:

$$\mu^\circ(x_1, ..., z_\nu) = \mu_r^\circ(x_1, ..., x_{N'-1}) - \beta^{-1}\ln\sum_{y\in s_\upsilon}\exp\left[-\beta\left((P_{N'}(y) + \sum_{i=1}^{N'-1} W_{i,N'}(x_i, y)\right)\right] \quad (11)$$

In this expression, the chemical potential no longer has a two-body additive form. The reason is that some other site can "polarize" the merged, equilibrated site altering its interaction with a third site. For a small number of sites, this presents no problem and eq 11 can be used directly. However, for more general use, it is desirable to recapture a two-body additive form by introducing approximations. We would like to find P' and W' such that

$$P'_{N'}(z_\nu) + \sum_{i=1}^{N'-1} W'_{i,N'}(x_i, y) \simeq -\beta^{-1}\ln\sum_{y\in s_\upsilon}\exp\left[-\beta\left((P_{N'}(y) + \sum_{i=1}^{N'-1} W_{i,N'}(x_i, y)\right)\right] \quad (12)$$

The P term reflects the intrinsic properties of the site without interactions with other sites, so putting all W and W' to zero gives

$$P'_{N'}(z_\nu) = -\beta^{-1}\ln\sum_{y\in s_\upsilon} \mathrm{e}^{-\beta P_{N'}(y)} \quad (13)$$

We now introduce the approximation that the interaction between the merged site and site i is not influenced by any other site, which implies setting the $W_{j,N'}$ with $j \neq i$ to zero:

$$P'_{N'}(z_\nu) + W'_{i,N'}(x_i, y) = -\beta^{-1}\ln\sum_{y\in s_\upsilon}\exp\left[-\beta(P_{N'}(y) + W_{i,N'}(x_i, y))\right] \quad (14)$$

Equations 13 and 14 together determine the P' and W'. This approximation depends on the merged site not being strongly polarized by more than one other site.

Because conformational change can cause closely clustered ionizable groups to come apart, sites that were merged in one conformer may not be in another, and if the "site" in question is comprised of internal water molecules, even the site may disappear on conformational change. That is, sites can be created, destroyed or have their number of available states changed upon conformational change. This presents no real difficulty as long as protons are properly accounted for. Here this is done in the way most consistent with the simple transition rules given above—elementary conformational transitions are restricted to those that do not change the number of bound protons in any site.

Solution and Analysis. The master equation, eq 1, can be written in matrix form as

$$\frac{\mathrm{d}\boldsymbol{p}}{\mathrm{d}t} = \boldsymbol{R}\boldsymbol{p} \quad (15)$$

where $\boldsymbol{R}$ is a matrix representing the transition possibilities and associated rate constants and $\boldsymbol{p}$ is the vector of microstate populations. Its solution is expected to have the familiar form

$$p_i = p_i^{\mathrm{eq}} + \sum_{j=1}^{N_{\mathrm{m}}-1} c_j E_{ij} \mathrm{e}^{\lambda_j t} \quad (16)$$

where the λ_j are the eigenvalues of $\boldsymbol{R}$, $\boldsymbol{E}$ is a matrix whose columns are the corresponding eigenvectors, $\boldsymbol{p}^{\mathrm{eq}}$ is the equilibrium distribution (which is also the zero eigenvector), and c_j are chosen to satisfy the initial condition. One expects the λ_j to be real and negative. However, this formulation suffers from

numerical problems, such as the generation of non-physical complex eigenvalues using general-purpose eigensolvers either when when attempting to include large numbers of states or when the rates span many orders of magnitude, as can happen if state energies span several tens of kT. Such problems can sometimes be alleviated by omitting states with energies higher than a chosen cutoff relative to the initial state, but a more robust method was desired.

Since the rate matrix $\boldsymbol{R}$ defined by eq 3 is not symmetric, it is not obvious that its eigenvalues are real; however, detailed balance allows for the construction of an equivalent symmetric eigenproblem by a similarity transformation[49,58,59] according to

$$\rho = \boldsymbol{S}p \qquad \boldsymbol{B} = \boldsymbol{SRS}^{-1} \tag{17}$$

where $S_{ii} = (p_i^{\mathrm{eq}})^{-1/2}$. The symmetry of $\boldsymbol{B}$ can by verified using eq 3, and the elements of $\boldsymbol{B}$ can be written explicitly as

$$B_{ij} = (p_i^{\mathrm{eq}})^{-1/2} R_{ij} (p_j^{\mathrm{eq}})^{1/2} = \frac{\kappa_{ij}}{e^{\beta\Delta G_{ij}/2} + e^{-\beta\Delta G_{ij}/2}} \tag{18}$$

Because the symmetry of $\boldsymbol{B}$ is manifest, it can be constructed from the ΔG without numerical errors spoiling its symmetry, and eigensolvers specialized for symmetric matrices can be employed. Moreover, the exponential dependence of elements of $\boldsymbol{B}$ is on $\Delta G/2$ rather than ΔG, so the range of order of magnitude of the matrix elements is reduced.

The above methods produce the time-dependent distributions, which themselves do not provide direct information about the direction of proton flow, efficiency of pumping, etc. However, an analysis of the flow of probability and protons can be constructed. The instantaneous flux of probability from state j to state i is given by the terms on the right-hand side of eq 1, and the net flux between them over the course of the photocycle is

$$F_{ij} = \int_0^\infty (R_{ij}\, p_j(t) - R_{ji}\, p_i(t))\, \mathrm{d}t \tag{19}$$

These can be calculated analytically from the exponential form of the solution of the master equation. The net release of a proton to one side, or uptake from the other during the photocycle, can be found by summing the net fluxes of all the transitions that involve the desired release or uptake.

3. bR Model and Computations

The only proton-binding sites included in the model are those known to be on the proton-transport pathway: Asp96, the lysine−retinal Schiff base (SB); Asp85; and a release group (RG) on the extracellular side. RG is a merged site formed from residues Glu194 and Glu204 in all conformers except the resting state. In the resting-state conformer, a pair of hydrogen-bonded water molecules that can accept a proton to become $H_5O_2^+$ is included in RG as well as Glu194 and Glu204. The existence of an excess proton in an hydrogen-bonded water network in the resting-state release group is supported by spectroscopic evidence[46,60−62] and our prior modeling work,[35] from which we draw our present treatment of the resting-state RG. RG is assumed to be in rapid internal equilibrium, and its interactions with other sites are treated by the approximation (eq 14). The ionization states of some near-pathway residues are fixed in their known ionization states: Asp115, protonated; Asp212, deprotonated; Arg82, protonated. All other acidic residues were fixed deprotonated, while all other Tyr, Arg, and Lys residues were fixed protonated. The conformational states included are those of the resting state (BR) and the intermediates M, N, and O. Prior to merging, the three subsites of the release group in the BR conformer would have 2^3 protonation states, but the rapid equilibrium treatment reduces this to four states with proton numbers 0 through 3. This and the three ordinary sites give the BR conformer $2^3 \times 4 = 32$ protonation states. Similarly RG in the M, N, and O conformers has three states (proton numbers 0, 1, and 2), which together with other sites gives 24 protonation states. The overall number of conformation/protonation microstates is then 104.

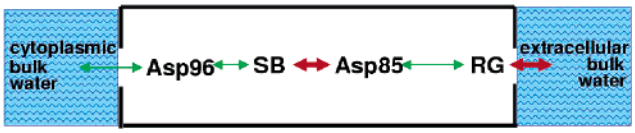

Figure 2. Access rules and classification for proton-transfer steps. Thick red arrows indicate transfers classified as fast while thin green arrows indicate transfers classified as slow. No other site−site or site−bulk transfers are allowed. Note that only one of the internal proton transfers, that between the Schiff base and Asp-85, is considered fast. Also, proton transfers between the bulk and either of these two bases are not allowed.

Site−site proton transfers, as elementary steps, are only allowed between sites that are accessible to one another, and site−bulk exchange is only allowed for sites accessible to either the extracellular or cytoplasmic bulk. The presumed accessibilities, adapted from ref 48 and shown in Figure 2, are based on proximity in the protein structure and their role in the proton-transfer pathway. For the purpose of assigning relaxation rates, they are classified as "fast" or "slow" depending on relative accessibility and distance. Each of the allowed transfer paths in Figure 2 generates a number of microstate−microstate transitions to be represented by rate-matrix elements (e.g., a transfer from SB to Asp85 may occur in different conformers, with other sites in different states, etc., thus generating numerous elements of $\boldsymbol{R}$).

All conformational changes among the M, N, and O are allowed as well as the interconversions N ↔ BR and O ↔ BR. These conformational changes can occur in any protonation state with the following proviso: When SB is deprotonated, no interconversions can occur between states with a 13-*cis* retinal (M and N) and those with a 13-*trans* retinal (BR and O). This reflects the much higher isomerization barrier in the deprotonated state.[63] The direct interconversion M ↔ BR is disallowed on the basis that a barrier requiring photoexcitation to surmount lies between them, and our simulations start with this barrier already crossed in the M → BR direction.

The $\mathrm{p}K_{\mathrm{int}}$ and, with one exception, the W_{ij} values needed for the calculation of the relative free energies of protonation states through eqs 8 and 9 were taken from our earlier work,[48] where the calculations and modeling are described in detail. Briefly, the MEAD computer programming suite[43,64] was used to calculate these values on the basis of a macroscopic electrostatic model that divided the protein, membrane, and water system into regions and treated each region as a medium of different dielectric constant, ϵ. The protein interior and membrane interior were given $\epsilon = 4$; the membrane headgroup region $\epsilon = 20$, bulk water $\epsilon = 80$, and an ionic strength of 0.1 M. Coordinates for the BR and M conformers were taken from PDB[65,66] entries 1C3W[19] and 1F4Z,[23] respectively. A minimal N model was made from the M

(58) Frankcombe, T. J.; Smith, S. C. *J. Comput. Chem.* **2000**, *21*, 592−606.
(59) Frankcombe, T. J.; Smith, S. C. *J. Theor. Comput. Chem.* **2003**, *2*, 179−191.
(60) Zscherp, C.; Schlesinger, R.; Tittor, J.; Oesterhelt, D.; Heberle, J. *Proc. Natl. Acad. Sci. U.S.A.* **1999**, *96*, 5498−5503.
(61) Wang, J.; El-Sayed, M. A. *J. Phys. Chem. A* **2000**, *104*, 4333−4337.
(62) Garczarek, F.; Brown, L. S.; Lanyi, J. K.; Gerwert, K. *Proc. Natl. Acad. Sci. U.S.A.* **2005**, *102*, 3564−3569.
(63) Tavan, P.; Schulten, K.; Oesterhelt, D. *Biophys. J.* **1985**, *47*, 415−430.
(64) Bashford, D. An object-oriented programming suite for electrostatic effects in biological molecules. In *Scientific Computing in Object-Oriented Parallel Environments*, Vol. 1343; Ishikawa, Y., Oldehoeft, R. R., Reynders, J. V. W., Tholburn, M., Eds.; Springer: Berlin, 1997.
(65) Abola, E. E.; Sussman, J. L.; Prilusky, J.; Manning, N. O. *Methods Enzymol.* **1997**, *277*.

Table 1. Relative Conformational Energies[a]

state transition	energy (kcal/M)
M:1010 → N:0110	0.72
N:0110 → O:1110	−0.65
O:1110 → BR:1101	−7.89

[a] Protonation state is indicated by a binary code where 0 is deprotonated and 1 is protonated and the digits (from left to right) represent Asp96, SB, Asp85, and RG. Data from ref 68.

structure through molecular mechanics simulations that altered the region near Asp96. The O model is a hybrid based on the M state in the RG region and the resting-state structure of the D85S mutant[27] (PDB code 1JV7), which is thought to be O-like in the SB-Asp85 region. The chosen set of conformers is not intended to be definitive, rather the small number of conformational states is intended to provide a minimal model of the conformation/protonation master-equation type outlined here. It would be of interest in future work to expand the conformational possibilities by adding more recent structures, such as the late-N model from the V49A mutant[31] and the acid blue form of the wild-type resting state, which like the D85S mutant, is considered a model of the O intermediate.[67]

The original pK_{int} and W_{ij} from ref 48 predict that in the M conformer, the driving free energy for the transfer of a proton from SB to Asp85 is only $\approx$ 0.2 kT. Such a small value suggests that the proton transfer would be incomplete, which is not the case experimentally. Moreover, calculations by Song et al.,[47] which include side chain conformational changes along with macroscopic electrostatics, find an energy difference of $\approx$ 4 kT. In light of this discrepancy and our belief that the energies calculated by Song et al. are more correct, we reduced the Asp85-SB W_{ij} term from 13.6 kT to 9.6 kT, which brings the energy difference for the proton transfer to $\approx$ 4 kT. The effect of this energy difference is discussed in section 4.

The relative energies between different conformational states are derived from the experimental work of Ludmann et al.[68] These energies are used as shown in Table 1 where it is assumed that the spectroscopic BR, M, N, and O states characterized by Ludmann et al. are purely in their conventional protonation microstates: that is, (using the binary notation of the table) BR in 1101, M in 1010, N in 0110, and O in 1110. The M to N energy shown is from the measurement of M_2 to N (the energies relative to M_1 were not measured). These three measurements are sufficient to determine the relative values of the $E_g(c)$ terms in eq 5.

The relaxation rates κ needed to determine the values of the rate-matrix elements through eq 4 are assigned according to transition category. The fast proton transfers are assigned κ_f, the slow are assigned κ_s, and conformational transitions are assigned κ_c. These three κ values are treated as free parameters of the model.

An implementation of the model, including the construction of microstates, transitions based on rules regarding elementary steps, and translation of MEAD pK_{int} and W_{ij} data into the needed energy differences was implemented in the Python programming language.[69] The extension package, Numeric Python,[70] which contains an interface to LAPACK,[71] was used for matrix operations. For the eigenproblem, the Numeric Python function used was eigenvectors, which calls the high-level LAPACK routine DGEEV to obtain eigenvalues and eigenvectors. Many of the numerical computations, including the eigenproblem solution were implemented redundantly in *Mathematica*. All values were verified at the level of double precision accuracy on a 32-bit processor. Calculation of integrated fluxes (eq 19) from the solutions was also implemented in Python, and the program GraphViz[72] was used to visualize these fluxes in the form of a directed graph.

4. Results

The equilibrium properties of systems of ionizable groups that are energetically coupled to each other is not adequately characterized by the concept of pK_a, which strictly speaking, applies only to the titration of sites not coupled to other sites that titrate in a similar pH range.[43,73] We therefore present results mainly in terms of the energy levels of the various states, as in our previous work.[48]

Figure 3 shows the calculated relative free energies of the individual microstates with protonation states represented according to Scheme 1. We also use a completely analogous binary notation in the text to refer to specific microstates. Our notation has the form conformer:protonation state, where 1 and 0 represent protonated or deprotonated sites, corresponding to the filled and open circles of Scheme 1. For example, O:1101 would refer to a microstate of the O conformer with Asp-96, the Schiff base, and the Release Group protonated, and Asp-85 deprotonated.

In some cases, pK_a-like values can be extracted from the energy differences displayed in Figure 3, but caution is needed particularly in interpreting pK_a differences as driving energies for proton transfers. For example, the process of adding a proton to Asp85 in the resting state, BR:1101 → BR:1111, has a ΔG of 7.3 kT at pH 7.0. Since this process adds one proton to the system, its ΔG depends on pH through a term, $+2.3\ kT\ \Delta$pH. Since $\Delta G = 0.0$ at the titration midpoint, $\Delta G_{pH=7} = -2.3\ kT\text{-}(pH_{mid} - 7.0) = 0$ leading to pK_a = pH_{mid} = 3.8. Similarly the ΔG for starting from the resting state and removing the SB proton, BR:1101 − BR:1001 is 6.3 kT, and since this process removes one proton, the pK_a value is 13.3. If one now attempts to calculate the free energy of moving a proton from SB to Asp85 through the difference of these two pK_a values, one obtains $2.3\ kT\ (13.3 - 3.8) = 21.8\ kT$. However, the correct value from Figure 3 for the BR:1101 → BR:1011 transition is 4.0 *kT*. The problem with the pK_a differencing procedure is that it double-counts the electrostatic interaction between Asp85 and SB.

At equilibrium, the model predicts the two most populous states to be the BR:1101 state (98%), the expected resting state of bR, and BR:1011 (1.7%). Interconversion between these two states occurs via the above-analyzed proton transfer between the Schiff base and Asp-85. To our knowledge, a small fractional deprotonation of the Schiff base in the resting state has not been detected experimentally. Visible absorbance measurements have found that Asp85 and SB are both protonated in 0.45% of molecules in the resting state,[74] but the present calculations give only 0.08% of molecules in such states, the lowest-energy such

(66) Abola, E. E.; Bernstein, F. C.; Bryant, S. H.; Koetzle, T. F.; Weng, J. Protein data bank. In *Crystallographic Databases—Informaton Content, Software Systems, Scientific Applications*; Allan, F. H., Bergerhoff, G., Sievers, R., Eds.; Data Comminssion of the International Union of Crystallography: Bonn/Cambridge/Chester, 1987.
(67) Okumura, H.; Murakami, M.; Kouyama, T. *J. Mol. Biol.* **2005**, *351*, 481−495.
(68) Ludmann, K.; Gergely, C.; Váró, G. *Biophys. J.* **1998**, *75*, 3110−3119.
(69) Beazley, D. *Python Essential Reference*, 2 ed.; New Riders: Indianapolis, 2001; see also http://www.python.org.
(70) Ascher, D.; Dubois, P. F.; Hinsen, K.; Hugunin, J.; Oliphant, T. Numerical python. Lawrence Livermore National Lab: 2001; http://numeric.scipy.org.
(71) Anderson, E.; Bai, Z.; Bischof, C.; Blackford, S.; Demmel, J.; Dongarra, J.; Du Croz, J.; Greenbaum, A.; Hammarling, S.; McKenney, A.; Sorensen, D. *LAPACK Users' Guide*, 3rd ed.; Society for Industrial and Applied Mathematics: Philadelphia, 1999.
(72) Gansner, E. R.; North, S. C. *Software Pract. Exp.* **2000**, *30*, 1203−1233; http://www.graphviz.org.
(73) Onufriev, A.; Case, D. A.; Ullmann, G. M. *Biochemistry* **2001**, *40*, 3413−3419.
(74) Balashov, S. P.; Imasheva, E. S.; Govindjee, R.; Ebrey, T. G. *Biophys. J.* **1996**, *70*, 473−481.

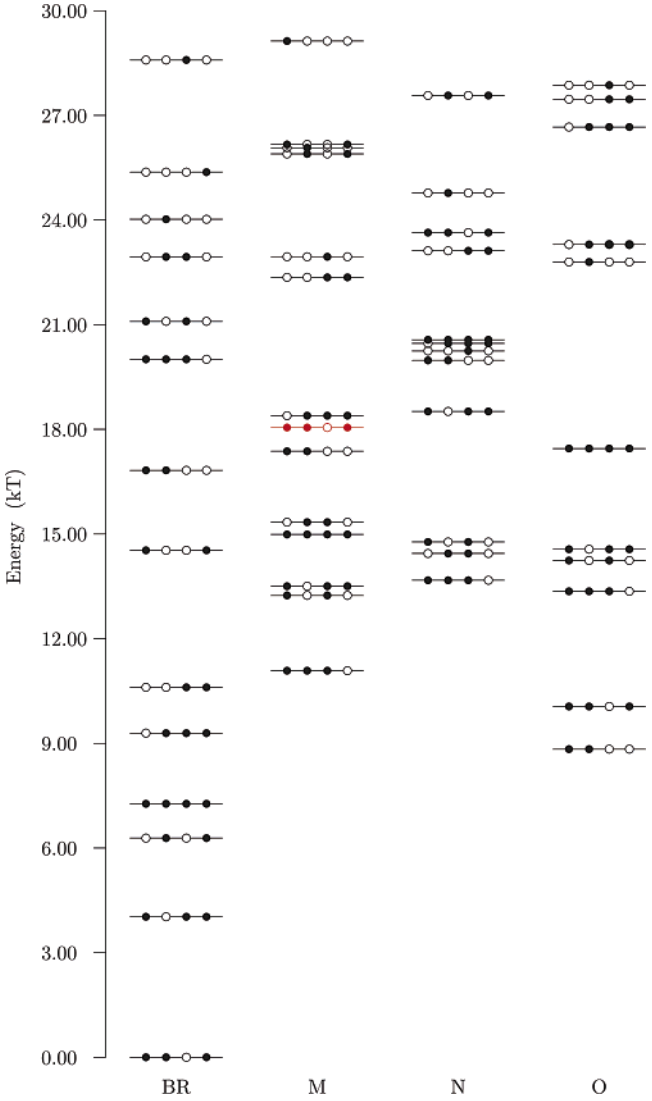

Figure 3. Energy diagram showing the microstate energies for the model. The conformer is given across the horizontal axis with the energy in kT (T = 300K) given on the vertical axis. Open circles indicate that the residue is deprotonated and filled circles indicate a protonated site. The circles correspond to Asp-96, the Schiff base, Asp-85, and the Release Group from left to right. The initial state, M:1101, is highlighted in red, and states above 30 kT are not shown.

Scheme 1

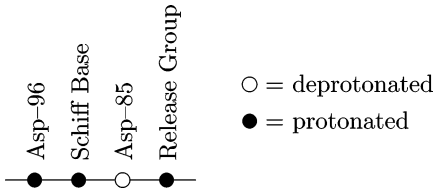

state being BR:1111 (the acid-blue state), whose energy level corresponds to a calculated pK_a for the acid-blue transition of 3.8 (see above). This prediction is somewhat high—a correct prediction of the experimental value of of 2.6[74] would require a higher blue-state energy, 10.1 kT, which would lead to an even smaller population of protonated Asp85 at pH 7.0. The calculations of Song et al.[47] similarly find a small amount of proton transfer from SB to Asp85 and/or Asp212 in the BR conformer, and among their reported microstate energies (Appendix III of their Supporting Information), the lowest energy state with both SB and Asp85 protonated is at 11.0 or 12.9 kT depending on whether nearby water is represented explicitly or as continuum. Balashov et al.[74] have proposed that the persistence of a small fraction of blue membrane in the pH 6−9 range, and its second titration at pK_a 9.7 is caused by a coupling of Asp85 and RG, such that deprotonation of RG raises the pK_a of Asp85 by 5.1 pK_a units (13.3 kT). Given the distance between these groups, it seems very unlikely that such a coupling can be purely electrostatic, and since the calculations of energies within the BR conformer are confined to purely electrostatic effects, it is understandable that very little blue-state protonation is seen. If the proposed SB−Asp85 coupling exists, it must be through local conformational changes that are not included in the present model. All other microstates account for less than 0.5% of the equilibrium population. States with more than one proton in the merged site RG are much too high in energy to appear with any significance either at equilibrium or in the kinetics and were excluded from further calculations leaving a 64-microstate model. Use of the approximation (eq 14) causes no significant changes in the microstate free energy differences.

In the other conformers, the lowest-energy protonation states are not necessarily those considered characteristic of the corresponding state; for example, M:1110, rather than M:1010, is the lowest-energy protonation state in the M conformer. As we have discussed previously,[48] the photocycle does not necessarily reach the lowest-energy protonation state if such states are not kinetically accessible. The real tests of the model then concern its kinetic consequences.

For photocycle kinetics, the free parameters of the model are the relaxation rates for conformational change, slow proton transfers ,and fast proton transfers; κ_c, κ_s, and κ_f, respectively. The relaxation rates for proton-transfer steps are assumed not to change with conformation; therefore, no "accessibility switch" is present in the model. Their effects were surveyed over a wide range of values. The sensitivity of pumping efficiency to variations of these parameters can be explored in a space of only two parameters, κ_s/κ_f and κ_c/κ_f, since the choice of κ_f sets the overall time scale and does not affect efficiency. The model was constructed and solved with values of both of these ratios ranging from 1 to 10^{-4}.

The efficiency of pumping for each model was determined by the net flux of proton release from RG, the only group directly accessible from the extracellular side. This was calculated as the sum of the integrated proton fluxes (eq 19) for all transitions in which RG exchanges a proton with the bulk. These values are presented as a log−log plot in Figure 4a, where zero corresponds to no pumping, and one corresponds to one proton transport per photocycle. (Choosing the flux between Asp96 and the cytoplasmic side as the measure of efficiency gives identical results to within 0.003.) These values can be regarded as a measure of the pumping efficiency of the LM to BR portion of the photocycle, that is, losses of efficiency due to failure to pass from photoexcitation to LM are not included.

Two broad triangular plateaus, one with no pumping and one with ~0.8 protons pumped (maximum 0.86), are separated by the diagonal defined by $\kappa_c/\kappa_s = 1$. Another edge of the high-efficiency plateau is defined by the value of κ_s/κ_f. In order to obtain a reasonably efficient photocycle, the intuitively expected relationship $\kappa_c < \kappa_s < \kappa_f$ must hold. More specifically $\kappa_s/\kappa_c \geq$

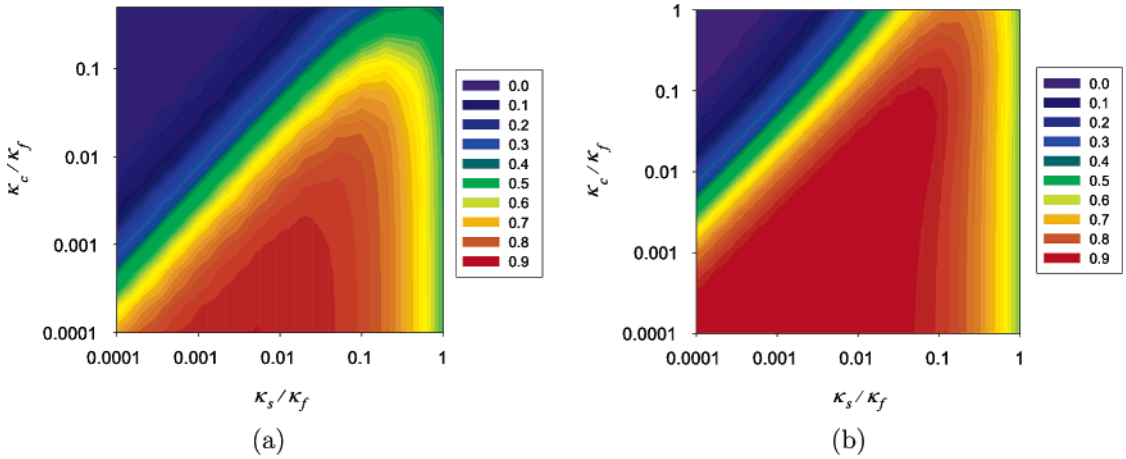

Figure 4. Fractional number of protons pumped per photocycle, calculated as the sum of the net integrated fluxes (eq 19) of all transitions in which a proton is released to the extracellular side. (a) The original model. (b) A model in which 13-*cis* ↔ all-*trans* is only allowed if Asp85 is protonated.

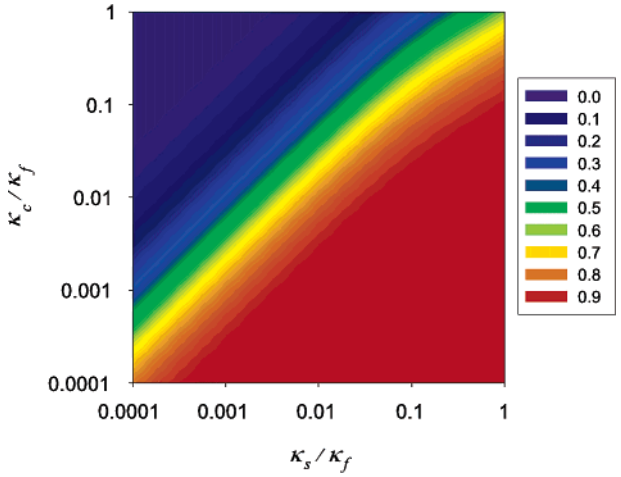

Figure 5. Fraction of 13-*cis* → all-*trans* isomerization during which Asp85 is protonated in the original model.

1 and $\kappa_f/\kappa_s \geq 5$ are sufficient to ensure a pumping efficiency of at least 0.7. Within these boundaries, pumping efficiency is relatively insensitive to variation of these parameters.

It has been shown experimentally that the rate of dark adaptation of bR, which involves an all-*trans* to 13-*cis* isomerization of the retinal, is at least 10^4 times slower when Asp85 is deprotonated than when it is protonated; and on this basis it has been proposed that Asp85 protonation may also be a requirement for re-isomerization from 13-*cis* to all-*trans* late in the photocycle. We therefore determined fraction of 13-*cis* to *trans* isomerization during which Asp85 is protonated in our model. This was calculated as the sum of the net integrated fluxes of all conformational changes between one of the *cis* conformers, M or N, and one of the *trans* conformers, BR or O, that occurs with Asp85 protonated. The results, shown in Figure 5, are that throughout the region in which $\kappa_s/\kappa_c \geq 1$ (lower right triangle in plot) nearly all the isomerization occurs with Asp85 protonated even though nothing has been put in the model to enforce this. This region of parameter space corresponds approximately to the high-efficiency plateau of Figure 4a. However, as κ_s/κ_c becomes smaller than one, the fraction of 85-protonated isomerization falls off in a manner almost identical to the falloff of pumping efficiency in this region of parameter space. One is led to speculate that if Asp85-protonation were made a prerequisite for isomerization, the efficiency of pumping might improve. To test this, a model was prepared in which this new isomerization rule is enforced, in addition to the original rule that the SB itself has to be protonated. The pumping efficiencies calculated from it are shown in Figure 4b, where comparison to Figure 4a shows that the new rule extends the boundary of the high efficiency region to approximately $\kappa_s/\kappa_c \geq 0.1$. The maximum pumping efficiency achieved is only increased slightly: 0.91 versus 0.86.

A similar proposal has been made for Asp96.[75,76] We find that in our original model whose only requirement for isomerization is protonation of SB, essentially all *cis* → *trans* isomerization occurs in states having Asp96 protonated, and that enforcing this as an isomerization requirement has no effect on efficiency (data not shown). The reason is that in the O conformer, all states with Asp96 deprotonated are high in energy (Figure 3), so transitions into them become very unfavorable. Thus protonation of Asp96 becomes a prerequisite for the transition into O without any such explicit requirement in the model.

For comparison of predicted time courses of microstate populations to time-resolved absorption data, the microstates were grouped according to their likely spectroscopic appearance, which is determined mainly by the conformation and ionization state of retinal and Asp85. States having all-*trans* retinal (the BR and O conformers), a protonated SB, and a deprotonated Asp85 were designated BR-like. States having all-*trans* retinal and both SB and Asp85 protonated are grouped as O-like. States having 13-*cis* retinal (the M and N conformers), SB deprotonated and Asp85 protonated are grouped as M-like. States having 13-*cis* retinal and both RG and Asp85 protonated are grouped as N-like. The initial state, which has a 13-*cis* retinal, a protonated SB, and deprotonated Asp85, is designated as LM-like. One exception to the above scheme was made for the sake of display: states with an O-like conformation and a BR-like protonation (i.e., SB protonated and Asp85 deprotonated) are grouped as OBR. Table 2 shows the relation of these groupings to the microstates that appear in significant population. It is notable that only 13 of the 64 possible microstates appear.

(75) Balashov, S. P.; Lu, M.; Imasheva, E. S.; Govindjee, R.; Ebrey, T. G.; Othersen, 3rd, B.; Chen, Y.; Crouch, R. K.; Menick, D. R. *Biochemistry* **1999**, *38*, 2026−39.
(76) Misra, S.; Govindjee, R.; Ebrey, T. G.; Chen, N.; Ma, J.-X.; Crouch, R. K. *Biochemistry* **1997**, *36*, 4875−4883.

Table 2. Sets of Microstates Used To Define the Spectroscopically Similar Groups

spectroscopic group	microstates
LM-like	M:1100, M:1101
M-like	M:1010, M:1011, N:1010
N-like	M:1110, M:0110, N:0110, N:1110
O-like	O:1110
OBR	O:1100, O:1101
BR	BR:1101

Calculated time courses for the various spectroscopically distinct groups are shown in Figure 6, panels A and B, which display the results of models with two different choices of κ_s/κ_f and κ_c/κ_f. Again, κ_f only sets the overall time scale and does not affect the ordering, magnitude, or relative timing of events. In both time courses the initial state (M:1101) decays rapidly into an M-like set of states followed by the rise of N-like states. The shape of the time course for the M-like states is characteristic of a biphasic system with the second, longer-lived set of states becoming evident as the less stable set forms the early N states. This feature is suggestive of the early M (M_1) and late M (M_2) states observed experimentally. The rise of BR overlaps O, OBR, and the decay of N. Despite the admittedly crude estimates of the relaxation rates for the elementary steps, the time courses for M, N, and the recovery of BR in Figure 6A show remarkable similarity to experimental results of Váró and Lanyi.[77] An overall time scale similar to experiment is obtained if $\kappa_f \simeq 0.25 \times 10^7\ s^{-1}$, in which case one would have $\kappa_s \simeq 0.25 \times 10^5\ s^{-1}$ and $\kappa_c \simeq 0.25 \times 10^4\ s^{-1}$. The main deviation from experiment is that the calculated O-like populations only rise to a barely detectable level between the third and fourth decade in time, while in place of O, the microstates we have grouped as OBR appear. These have an O-like conformation but a BR-like protonation state.

A detailed analysis of the pathway in terms of microstates and sequences of elementary events that lead to pumping or the lack of it can be obtained using some tools from graph theory. Figure 7 displays the system as a topological graph with the microstates as the vertexes (or nodes) and the set of allowed microstate transitions as the edges. The net flow of probability during the photocycle is displayed by attaching weights and directions to each edge according the direction and magnitude of the probability flux (eq 19) associated with the corresponding transition. Thus a weighted, directed graph is obtained and potential sequences of microstate transitions are viewed as pathways through the network, with the weights providing information about the extent to which different paths are followed. Since the transitions are specific with respect to proton transfer, the pumping or non-pumping character of particular pathways can be determined by inspection.

The conventionally expected sequence of events of the latter part of the bR photocycle can be seen in Figure 7. From the initial LM state at the top, proton transfer from SB to Asp85 and release of a proton from RG to the extracellular side occur, in either order (the four red edges near the top), to reach the microstate M:1010, which corresponds to the conventional M state. Since both processes are fast, they will appear to occur simultaneously. Inspection of the energy level diagram (Figure 3) shows that these steps are energetically downhill (4.8 *kT*). Although there is a lower-energy protonation state in the M conformer, M:1110, it is not directly accessible by an elementary step from M:1010, since there is no elementary step bringing a proton from the bulk directly to SB. This state is a local energy minimum in that all available transitions are uphill. The one with the smallest increase (1.5 *kT*) is a conformational transition to N (the red branch to the left). This leads, by a slightly downhill step, to the reprotonation of SB from Asp96, reaching the conventional N state, N:0110. The next step, also downhill, is reprotonation of Asp96 from the extracellular bulk while still in the N conformer followed by a slightly downhill transition to the O conformer (the left red branch rejoining the central branch) reaching the conventional O state, O:1110. Transfer of a proton from Asp85 to RG followed by a conformational change to BR, a steeply downhill pair of steps, recovers the resting state, BR:1101 to complete the photocycle with the net effect of transferring one proton across the membrane. The other two terminal states at the bottom of the graph are the states present in very small population at equilibrium (see above).

However, this conventional pathway is not the one followed by the greatest population—instead 58% of the flux follows the central path through the diagram which diverges from the conventional path after M:1010, the local energy minimum. The two competing steps from this point are the above-mentioned transition to the N conformer or the reprotonation of the Schiff base from Asp96 while still in the M conformer. The latter step is uphill by 2.1 kT, which is a larger energy increase than the former, but the relaxation rate for the proton transfer, κ_s, is faster than that for conformational change, κ_c. As indicated by the node-coloring in the graph the resulting state M:0110 would appear N-like in its visual absorption because SB has been reprotonated but retinal has not yet re-isomerized to the all-*trans* form. The deprotonation of Asp96 would also appear in the IR spectra of either M:0110 or N:0110. A downhill transition is now available by reprotonation of Asp96 from the cytoplasmic bulk to reach M:1110. At this point the conventional pathway is rejoined and the system proceeds through O to BR as described above. The N conformer is bypassed altogether. Like the conventional pathway this pathway also has the net effect of transferring one proton across the membrane.

Of course, there are many alternate pathways, some of which result in the net translocation of a proton and some of which are nonproductive. The vast majority of these pathways involve insignificant proton fluxes and are not shown in Figure 7. However, there are two significant nonproductive pathways that account for a loss of 0.128 protons out of the total 0.152 of lost efficiency. The largest of these involves protonation of Asp85 from RG (the thin red loop on the right). The path then rejoins the central branch, but there is no net pumping since the proton transfers involved are purely internal. This pathway followed by 0.095 of the ensemble. Although protonation of Asp85 from RG is energetically more favorable than its protonation from SB, the latter is a faster process than the former and is followed by a larger population, while only 0.095 of the population follows the non-pumping pathway. This is a possible explanation for the observation that κ_f must be significantly larger than κ_s for efficient pumping. The next-largest nonproductive pathway begins by diverging from the main pathway's M:1100 microstate. A conformational change from M to O (which involves re-isomerization of the retinal) brings the system to O:1100,

(77) Váró, G.; Lanyi, J. K. *Biochemistry* **1991**, *30*, 5008−5015.

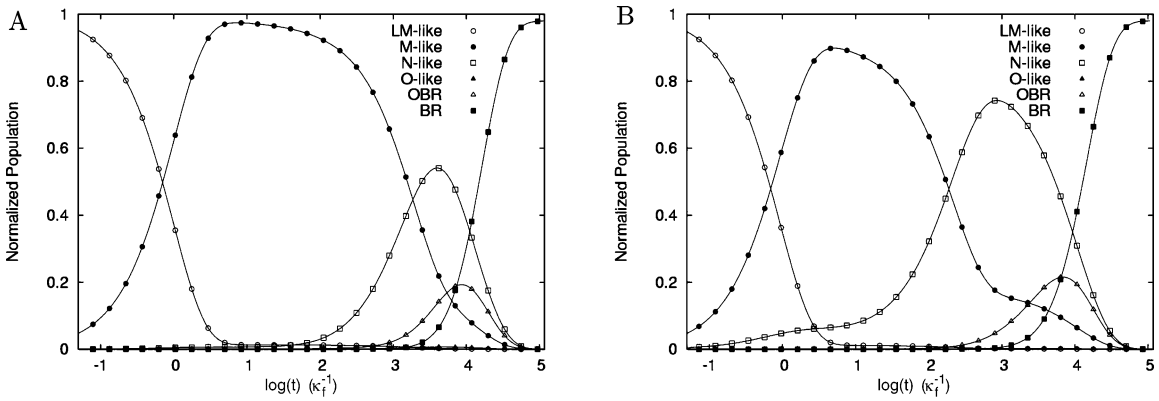

Figure 6. Calculated time courses from the model with the free energy levels of Figure 3 and selected relaxation rates, κ. Panel A corresponds to $\kappa_s/\kappa_f = 10^{-2}$ and $\kappa_c/\kappa_f = 10^{-3}$ and panel B to $\kappa_s/\kappa_f = 10^{-1}$ and $\kappa_c/\kappa_f = 10^{-3}$. The classification of microstates into spectroscopically similar groups is discussed in the text and the (arbitrary) time scale is set by κ_f. Compare panel A with experimental results of Figure 3A in ref 77.

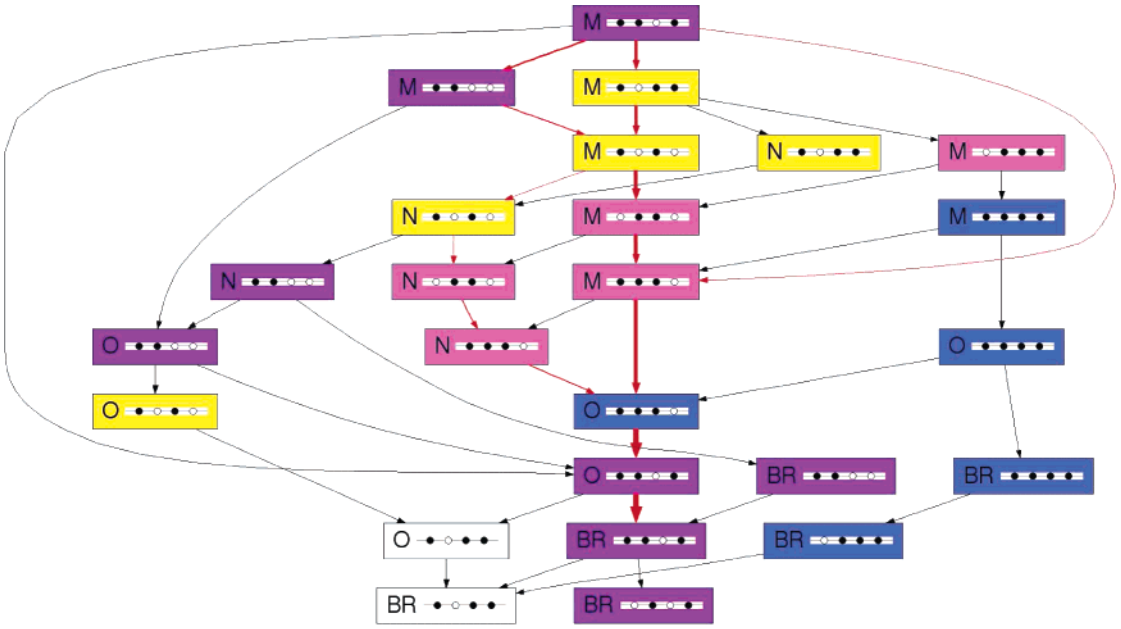

Figure 7. Probability flux diagram for the model with the energy levels of Figure 3 and the relaxation rates of Figure 6A. The boxes contain the names of the protein conformers and a pictorial representation of the protonation state as in Figure 3 and are colored by spectroscopic group (Table 2). Red lines indicate calculated fluxes with a magnitude of 0.075 or greater with the thickness of the lines indicating the relative magnitude of the fluxes. Fluxes less than 0.00125 are not shown. The diagram is organized with proton-pumping pathways down the center and nonproductive ones at the right and left sides (see text).

lowering its energy by 8.5 kT. This is followed by re-uptake of a proton from the extracellular side to RG, and then passage to the BR conformer with no net proton transport. This pathway is followed by only 0.033 of the population, because the conformational change to O competes with proton-transfer processes, and for these parameter values, even slow proton transfers are 10 times faster than conformational transitions. However, in the region of parameter space where κ_s/κ_c becomes less than 1 (upper left triangle in Figure 4a) the flux through this path increases and contributes significantly to the loss of efficiency (data not shown). This is one reason why imposing the restriction that Asp85 must be protonated for isomerization to occur extends the high-efficiency plateau partway into this region. A few other nonproductive pathways that account for even smaller fluxes can be seen in the graph, including a conformational transition directly from the initial state to the O conformer (leftmost black loop), bypassing proton transfer altogether, and a path through M:1111 (right side) in which SB is reprotonated from the "wrong" side.

As described in section 3, we have taken the energy drop associated with proton transfer from Asp85 to SB in the M state from the calculations of Song et al., who used macroscopic dielectric methods similar to ours, but included conformational flexibility.[47] Figure 8 shows the importance of this energy drop for the efficiency of pumping. Efficiency falls off rapidly as the gap is decreased from the 4.5 *kT* value used in the calculations discussed above. A flux diagram for a small gap model (diagram not included) shows increased flux through the nonproductive pathways discussed above, including the ones involving direct passage from the initial state to M:1110, direct conformational change from the initial state to O, and the divergence into O conformers from M:1100. The common cause is that a rapid initial equilibrium is established between states where the proton has been transferred from SB to Asp85 had those where it has not. Because of the small energy gap, the pre-transfer states are present at significant population, and it is these states from which the nonproductive pathways diverge from the productive ones.

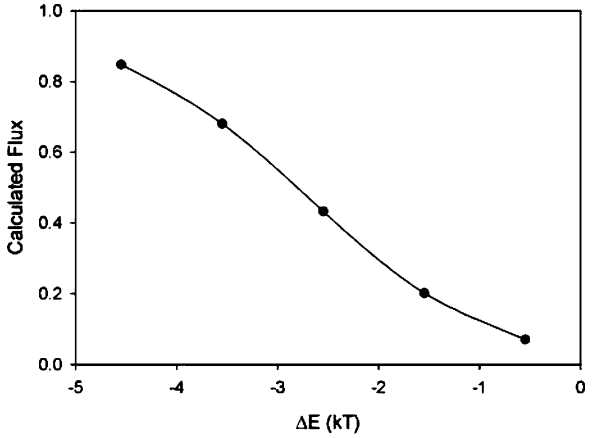

Figure 8. Calculated net proton transport as a function of the energy difference associated with proton transfer from the Schiff base to Asp-85 in the M conformer. Model parameters otherwise the same as for Figure 7.

Discussion

Using only three different relaxation rates is probably an oversimplification. One could expect that each of the five allowed proton transfers and each of the five allowed conformational changes could have different relaxation rates. Furthermore, conformational change in the region of a proton-transfer step might be expected to alter the relaxation rate of that step, leading to still more different relaxation rates. However, the limitation to three parameters makes feasible a thorough exploration of the model's sensitivity to their values. This exploration reveals broad regions of parameter space where proton pumping is not sensitive to parameter choice. Conformation-independent relaxation rates do not imply that observed exchange rates, such as H/D exchange, would be conformation independent, since the slower of the forward or backward rates would be much less than the relaxation rates in the case of a large energy difference between states (see section 2.1, and eq 4).

With respect to the function of bR, the most important result is that proton pumping can be achieved and that most of the kinetic features of the photocycle can be explained without an invoking an accessibility switch—that is, with no conformational dependence of the relaxation rates for the proton-transfer steps. Instead, the coupling of changes in the relative energies of different protonation states with the energetics of conformational change gives rise to vectorial proton motion along pathways that are always open, but not always energetically favorable. Thus an affinity-switch or local-access model[34] is sufficient.

The features of the relaxation rates needed for pumping are that the short-distance proton transfers, especially the proton transfer between SB and Asp85, have faster relaxation rates than either long-distance proton transfers or conformational changes and that the relaxation rate of conformational change be similar to or slower than that of long-distance proton transfers. A purely energetic feature that is also essential is the drop in energy associated with the transfer of a proton from SB to Asp85 in the M conformer. This, together with the rapid relaxation for short proton transfers sets up the microstate M:1010 (the conventional M state) as a local, low-energy trap into which the system rapidly falls, bypassing nonproductive paths, and from which the escape routes having the lowest energy barriers all lead to productive pathways. On a more macroscopic level, the requirement that this energy gap be relatively large implies that the passage from very early M or LM to late M (or M_2) be essentially irreversible, which is the case experimentally.[77] Furthermore, there are two important restrictions on conformational transitions important for efficient pumping. These are that the M conformer cannot directly return to BR and that changes in the isomerization state of the retinal 13 bond can only occur when SB is protonated (a feature of isomerization barriers within the Schiff-base retinal).

The master-equation model reproduces the essential features of the bR photocycle with the proper temporal ordering of events over a wide range of values for the relaxation rate parameters. A particularly encouraging aspect of the current model is its ability to reproduce most of the qualitative features of known experiments. A direct comparison of Figure 6A with time courses obtained from difference spectroscopy (Figure 3A in Váró and Lanyi[77]) demonstrates this quite clearly. The main disagreement with experiment is that where time-resolved visible absorption measurements detect O, a state in which the retinal chromophore has returned to its all-*trans* conformation and both the SB and Asp85 are protonated, our model predicts the rise of an OBR state, which has an O-like conformer but a BR-like protonation state. Inspection of the flux diagram (Figure 7) shows that the true O state is on the major pathway but never accumulates because the proton transfer from Asp85 to RG, although slow, is slower than the conformational transitions leading to O from either M or N. As described in section 3, the O model from which protonation state energies are derived is a hybrid of the Ser85 mutant structure, which is proposed to be O-like,[27] and an M structure. With this O model, a BR-like protonation state is lower in energy than an O-like one leading to the observed behavior of the model, and it may be that these energetics are incorrect due to deficiencies of the O model. Another possibility is the true relaxation rate of the Asp85-RG proton transfer is similar to or slower than the conformational change from O to BR. This would allow for a greater accumulation of O:1110, the conventional O state.

A surprising feature of the model is that most of the population bypasses the N conformation and achieves the reprotonation of SB from Asp96 while still in the M conformer. Although unexpected, this result is not necessarily inconsistent with experiment since the resulting M:0110 state has the important features of N: the reprotonation of SB from Asp96 and a 13-*cis* retinal. It is interesting that this reprotonation takes place even though it is uphill by 2.1 kT. The structural model for M that we have used is thought to be a late M state[23] and may already have significant N-like character, which would help explain why it can play the role of N in this model. Another surprise is the participation in productive pathways of states that have 13-*cis* retinal conformers but O-like protonation states. Such substates have been suggested previously on the basis of mutational studies of the photocycle.[76]

The model of conformationally coupled proton transport presented here is more fine-grained than that typically used in the assignment of states and rates for the fitting of spectroscopic data, in which one strives for the minimal model that fits the data, but more coarse-grained than molecular mechanics or QM/MM simulations of conformational changes and proton transfers, in which one strives to include as full atomic detail as computationally feasible. In exchange, it provides more specific

detail about key events of the functional cycle than the data-fitting models, and spans much more time than atomistic simulations. Because of the low computational cost of setting up and solving any one model (∼1 min in the present case) uncertainty in some parameters can be dealt with by exploration of the model's sensitivity to their values. This allows more rigorous techniques to be brought to bear on those parameters that matter most.

These methods are potentially applicable to any system in which proton transport is coupled to protein conformational changes, including both conformationally driven proton pumping, as in bR or, conformational changes driven by proton gradients, as in flagellar motors. The sites need not be confined to two states, protonated or deprotonated, but can be more complex, reflecting tautomerism and multiple ionization states. Binding of small ligands other than protons can be included by introducing new kinds of sites and the bulk chemical potentials of their ligands. This would enable simulation of co-transporters, such as the Na^+/H^+ anti-porter. Electrons can be treated formally as "ligands" for the study of coupled proton and electron transport, as in cytochrome oxidase.[78]

Acknowledgment. The authors acknowledge support from the National Institutes of Health through Grant GM45607 and from The American Lebanese Syrian Associated Charities, Inc. (ALSAC). In addition, we thank a reviewer who proposed Asp85 protonation as a prerequisite for retinal isomerization and Nicholas LaBello (University of Memphis) for a critical reading of the manuscript.

JA060742D

(78) Stuchebrukhov, A. A. *J. Theor. Comp. Chem.* **2003**, *2*, 91−118.